

PAPER • OPEN ACCESS

## Accumulation of stress induced martensite in $\text{Fe}_{43.5}\text{Mn}_{34}\text{Al}_{15\pm x}\text{Ni}_{7.5\mp}$ X shape memory alloys

To cite this article: V Apostol *et al* 2019 *IOP Conf. Ser.: Mater. Sci. Eng.* **572** 012032

View the [article online](#) for updates and enhancements.

# Accumulation of stress induced martensite in $\text{Fe}_{43.5}\text{Mn}_{34}\text{Al}_{15\pm X}\text{Ni}_{7.5\mp X}$ shape memory alloys

V Apostol<sup>1</sup>, N M Lohan<sup>1</sup>, E Mihalache<sup>1</sup>, R I Comănesci<sup>1</sup>, N Cimpoesu<sup>1</sup>, B Pricop<sup>1</sup>, M Popa<sup>1</sup> and L G Bujoreanu<sup>1,\*</sup>

<sup>1</sup> Faculty of Materials Science and Engineering, The “Gheorghe Asachi” Technical University of Iasi, Blvd. Mangeron, No. 69A, 700050, Iasi, Romania

E-mail: lgbujor@tuiasi.ro

**Abstract.**  $\text{Fe}_{43.5}\text{Mn}_{34}\text{Al}_{15}\text{Ni}_{7.5}$  shape memory alloys (SMAs), have drawn considerable attention from the part of scientific community due to its superelastic behaviour, stable over a large thermal range (from  $-50$  to  $+150^\circ\text{C}$ ) [1]. After cyclic heat treatment, solution treatment and ageing, the specimens became oligocrystalline and were reinforced by NiAl nanoprecipitates. The typical thermomechanical processing routine, before cyclic heat treatment of FeMnAlNi alloys, involves hot rolling, annealing and cold rolling [2]. The present paper discusses the effects of  $\pm 1.5$  at. % aluminium substitution with nickel, by correlating tensile behaviour with microstructural observations. The SMA specimens with chemical composition  $\text{Fe}_{43.5}\text{Mn}_{34}\text{Al}_{15\pm 1.5}\text{Ni}_{7.5\mp 1.5}$  were subjected to tensile tests, comprising loading-unloading cycles, based on which recoverable strain and energy storage efficiency were calculated. Considering that, in each cycle, a permanent strain was obtained, it follows that not all of the amount of stress induced martensite completely reversed to austenite, but a small part of it was accumulated in each cycle. By optical and scanning electron microscopy, the microstructural changes correlated with stress induced martensite accumulation were emphasized, while considering the effects of  $\pm 1.5$  at. % Al substitution with Ni.

## 1. Introduction

$\text{Fe}_{43.5}\text{Mn}_{34}\text{Al}_{15}\text{Ni}_{7.5}$  shape memory alloys (SMAs), experiencing superelastic strains over 12 % within a thermal range from  $-50$  to  $+150^\circ\text{C}$  (with negligible changes of the critical stress for martensitic transformation), have been developed since the beginning of the present decade, as potential candidates for superelastic, damping and sensor materials [1].

The superelastic behaviour of FeMnAlNi based alloys is caused by the reversible formation of  $\gamma'$ -face centred cubic (fcc) martensite, stress induced from an  $\alpha$ -body centred cubic (bcc) austenite, strengthened by coherent precipitation of ordered  $\beta$ -NiAl-bcc [2]. In addition, the superelastic behaviour is enhanced by the obtainment of oligocrystalline structure characterized by the absence of triple junctions between grains, which improves the reversibility and suppresses grain boundary constraints during loading [3]. The superelastic behaviour involves the presence of one obvious stress plateau or an inflection point, on the unloading path of a loading-unloading curve [4] which can cause recoverable strains as large as 25 % [5].

The superelastic behaviour can be described by means of two parameters: (i) recoverable strain ( $\epsilon_{\text{rec}}$ ) and (ii) energy storage efficiency ( $\eta$ ). These parameters are described as follows:



$$\varepsilon_{rec} = (\varepsilon_t - \varepsilon_p) / (\varepsilon_t - \varepsilon_0) \times 100 \quad (1)$$

Where  $\varepsilon_t$  – total strain;  $\varepsilon_p$  – permanent strain;  $\varepsilon_0$  – initial strain.

$$\eta = E_2 / E_1 \times 100 \quad (2)$$

Where  $E_1$  – total energy consumed on loading, proportional to the area under the loading curve and  $E_2$  – unloading-released energy, proportional to the area under the unloading curve [4].

In the case of an ideally superelastic SMA, stress induced martensite is fully reversible and no permanent strain ( $\varepsilon_p$ ) is obtained. However, in actual cases, there is always an amount of permanent strain which accumulates with the increase of the number of cycles. This gradual increase of permanent strain is equivalent to an amassment of stress induced martensite which no longer transforms to austenite during mechanical cycling.

The present paper aims to evaluate the effects of  $\pm 1.5$  at. % Al substitution with Ni within  $\text{Fe}_{43.5}\text{Mn}_{34}\text{Al}_{15\pm 1.5}\text{Ni}_{7.5\mp 1.5}$  SMAs, upon the accumulation of untransformed stress induced martensite. In this purpose, the evolution of recoverable strain and energy storage efficiency will be correlated with the successive microstructural changes observed during thermomechanical processing, by optical and scanning electron microscopy.

## 2. Materials and methods

Three ingots, with chemical compositions  $\text{Fe}_{43.5}\text{Mn}_{34}\text{Al}_{16.5}\text{Ni}_6$ ,  $\text{Fe}_{43.5}\text{Mn}_{34}\text{Al}_{15}\text{Ni}_{7.5}$  and  $\text{Fe}_{43.5}\text{Mn}_{34}\text{Al}_{13.5}\text{Ni}_9$ , respectively, were subjected to the following thermomechanical processing routine [6]: (i) melting in a cold crucible induction furnace; (ii) casting into copper moulds; (iii) rough machining to cylindrical shapes; (iv) longitudinal cutting by wire spark erosion; (v) hot rolling at  $1060^\circ\text{C}$ ; (vi) annealing at  $900^\circ\text{C}$ / 1h/ water quenching and (vii) cold rolling with up to 92 % thickness-reduction.

“Dog bone” specimens were cut, by wire spark erosion, with gauge dimensions of  $3 \times 2 \times 0.7$  mm<sup>3</sup>. Tensile loading-unloading cycles were applied on an INSTRON 3382 testing machine with a crosshead displacement rate of 0.5 mm/ min. The surface areas under the loading ( $E_1$ ) and unloading ( $E_2$ ) curves were calculated. For each cycle, the values of recoverable strain and energy storage efficiency were determined.

Samples of each of the three above mentioned processing state, hot rolling, annealing and cold rolling, were metallographically prepared for optical microscopy (OM) and scanning electron microscopy (SEM), the latter including energy dispersive spectroscopy (EDS). For OM, the specimens were ground, polished and etched with a solution of 8.5 % vol  $\text{CuSO}_4$ , 8.5 % vol  $\text{H}_2\text{O}$ , 33 % vol  $\text{CH}_3\text{-CH}_2\text{-OH}$  and 50 % vol, after being heating to about  $50^\circ\text{C}$  with a hot-air gun. For SEM, samples were ground down to 5  $\mu\text{m}$  grit size and finally vibration-polished using colloidal  $\text{SiO}_2$  suspension with 0.02  $\mu\text{m}$  particle size.

## 3. Experimental results and discussion

### 3.1 Tensile cycling

The loading-unloading curves, recorded with the three types of specimens in cold rolled state, up to the maximum strain of 4 %, are summarized in Figure 1.

It is noticeable that the specimen  $\text{Fe}_{43.5}\text{Mn}_{34}\text{Al}_{15}\text{Ni}_{7.5}$ , from Figure 1(b), underwent a maximum stress with 75 % larger than the other two. The loop closed much quicker, at this specimen, since permanent strain  $\varepsilon_p$  increased only with 0.13 % in the 3<sup>rd</sup> cycle and 0.11 % in the 4<sup>th</sup>. At each of the three specimens under study permanent strain increased slower and slower, with the increase of the number of cycles, in such a way that a closed loop was obtained after five cycles. The shape of the tensile curves corresponding to  $\text{Fe}_{43.5}\text{Mn}_{34}\text{Al}_{16.5}\text{Ni}_6$ , from Figure 1(a) is different from the other two. In the 1<sup>st</sup> cycle two inflection points are noticeable, marked with orange and blue arrows, on the loading

and unloading portions of the curve. As mentioned above, any inflection point could correspond to a stress induced martensitic transformation. With increasing the number of cycles, only the lower-stress inflection point persists. The deformational and energetic parameters are summarized in Table 1.

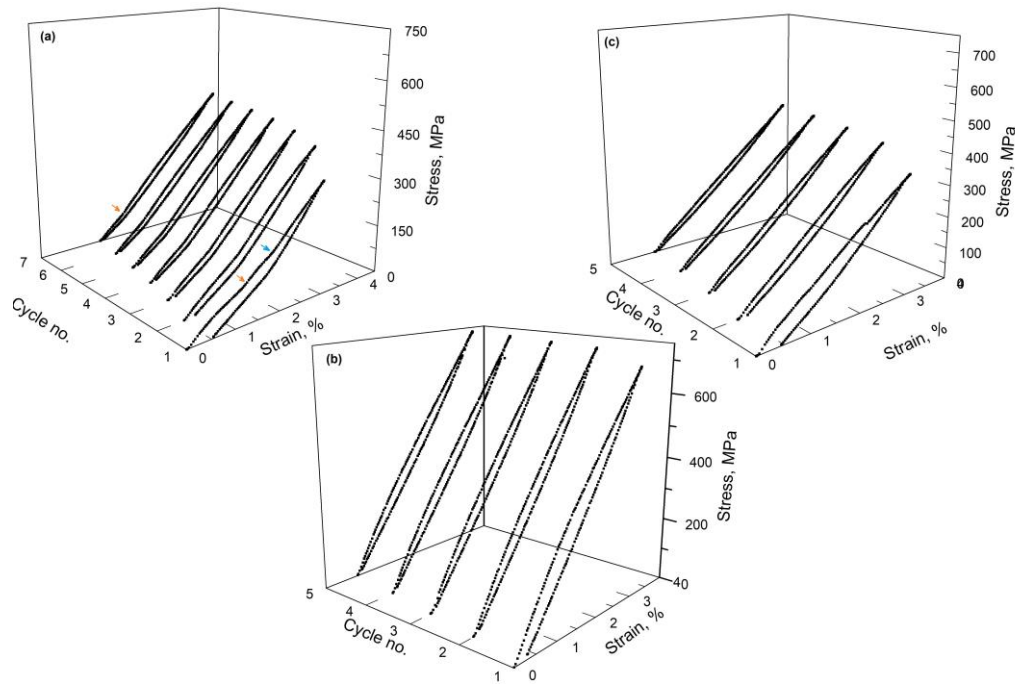


**Figure 1.** Tensile loading-unloading curves recorded during mechanical cycling, at specimens in cold rolled state, with different chemical composition: (a)  $\text{Fe}_{43.5}\text{Mn}_{34}\text{Al}_{16.5}\text{Ni}_6$ ; (b)  $\text{Fe}_{43.5}\text{Mn}_{34}\text{Al}_{15}\text{Ni}_{7.5}$  and (c)  $\text{Fe}_{43.5}\text{Mn}_{34}\text{Al}_{13.5}\text{Ni}_9$ .

**Table 1.** Summary of tensile parameters from Figure 1.

Alloy	Cycle no	$\epsilon_0$ , %	$\epsilon_t$ , %	$\epsilon_p$ , %	$E_1$ , MJ/m <sup>3</sup>	$E_2$ , MJ/m <sup>3</sup>
$\text{Fe}_{43.5}\text{Mn}_{34}\text{Al}_{16.5}\text{Ni}_6$	1	0	2.97	0.54	479	372
	2	0.54	3.55	0.79	593	499
	3	0.79	3.79	0.96	614	540
	4	0.96	3.97	1.1	634	566
	5	1.1	4.1	1.22	639	577
	6	1.22	4.23	1.34	655	589
	7	1.34	4.35	1.45	667	605
$\text{Fe}_{43.5}\text{Mn}_{34}\text{Al}_{15}\text{Ni}_{7.5}$	1	0	3.01	0.3	1136	933
	2	0.3	3.31	0.43	1173	1033
	3	0.43	3.44	0.56	1160	1038
	4	0.56	3.56	0.67	1167	1045
	5	0.67	3.68	0.78	1167	1045
$\text{Fe}_{43.5}\text{Mn}_{34}\text{Al}_{13.5}\text{Ni}_9$	1	0	3.01	0.45	585	453
	2	0.45	3.47	0.64	637	554
	3	0.64	3.64	0.76	642	576
	4	0.76	3.77	0.87	645	585
	5	0.87	3.87	0.97	645	593

Analysing these values enables to formulate the following observations:

- the specimen  $\text{Fe}_{43.5}\text{Mn}_{34}\text{Al}_{16.5}\text{Ni}_6$  enabled the largest total strain, 4.1 %, after 5 cycles;
- the specimen  $\text{Fe}_{43.5}\text{Mn}_{34}\text{Al}_{15}\text{Ni}_{7.5}$  enabled the lowest permanent strain, 0.78 % but required the highest amount of energy, 1167 MJ/m<sup>3</sup>, after 5 cycles;
- the 5<sup>th</sup> cycle became reproducible at specimens  $\text{Fe}_{43.5}\text{Mn}_{34}\text{Al}_{15}\text{Ni}_{7.5}$  and  $\text{Fe}_{43.5}\text{Mn}_{34}\text{Al}_{13.5}\text{Ni}_9$ , since loading-consumed energy,  $E_1$ , did not vary from the 4<sup>th</sup> to the 5<sup>th</sup> cycle.

Based on the parameters listed in table 1, the values of recoverable strain and energy storage efficiency were determined. Their evolution with the number of cycles is illustrated in Figure 2.

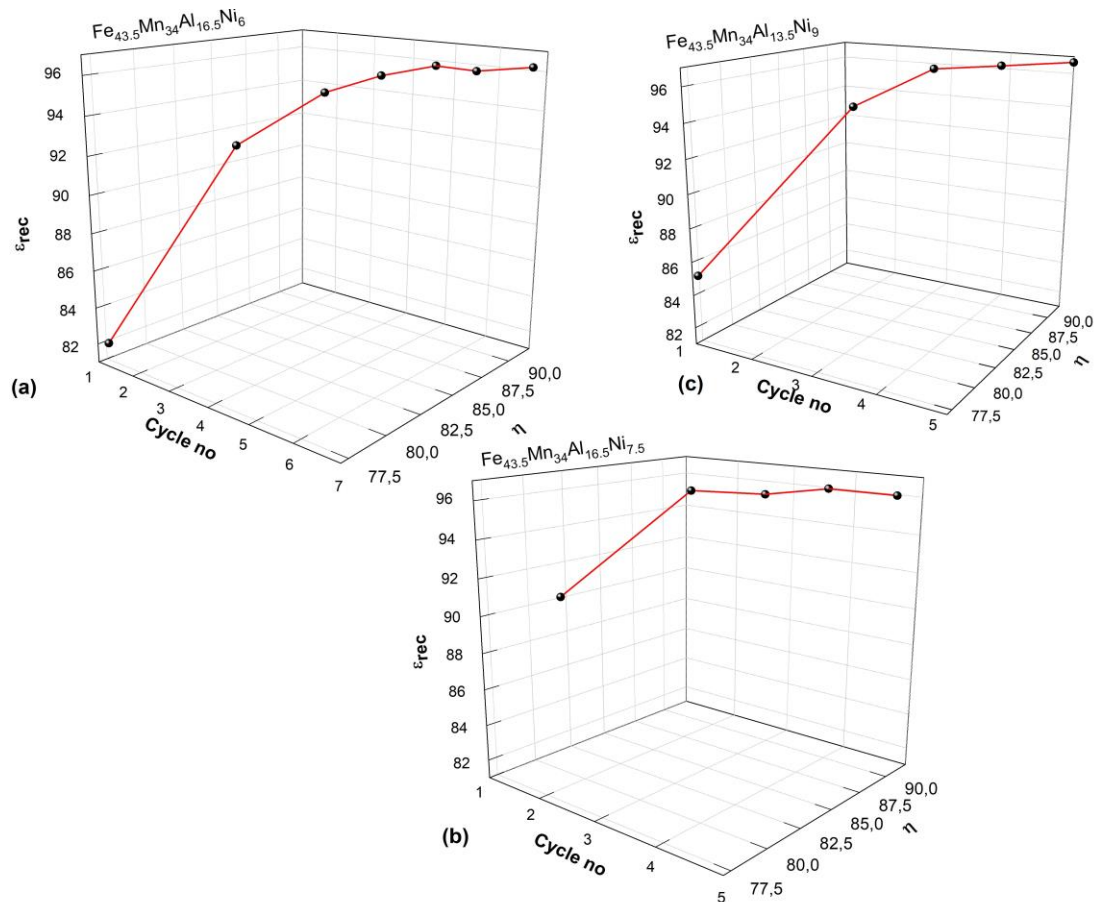


**Figure 2.** Variations of recoverable strain and energy storage efficiency with the number of mechanical cycles: (a)  $\text{Fe}_{43.5}\text{Mn}_{34}\text{Al}_{16.5}\text{Ni}_6$ ; (b)  $\text{Fe}_{43.5}\text{Mn}_{34}\text{Al}_{15}\text{Ni}_{7.5}$  and (c)  $\text{Fe}_{43.5}\text{Mn}_{34}\text{Al}_{13.5}\text{Ni}_9$ .

The variation range of energy storage efficiency,  $\eta$ , is the same for all the three alloys under study but the initial recoverable strain is much larger at  $\text{Fe}_{43.5}\text{Mn}_{34}\text{Al}_{15}\text{Ni}_{7.5}$ , in contrast to the other two. This difference is in good agreement with the higher maximum stress underwent by this specimen. Considering the values of permanent strain, from table 1, it is expectable that the specimen  $\text{Fe}_{43.5}\text{Mn}_{34}\text{Al}_{16.5}\text{Ni}_6$  to accumulate the highest amount of untransformed stress induced martensite.

### 3.2 Microstructural analysis

After hot rolling and annealing, oxygen contamination was noticed at the edge of the specimens but did not exceed 100  $\mu\text{m}$  in depth, as demonstrated by the EDS profiles summarized in Figure 3.



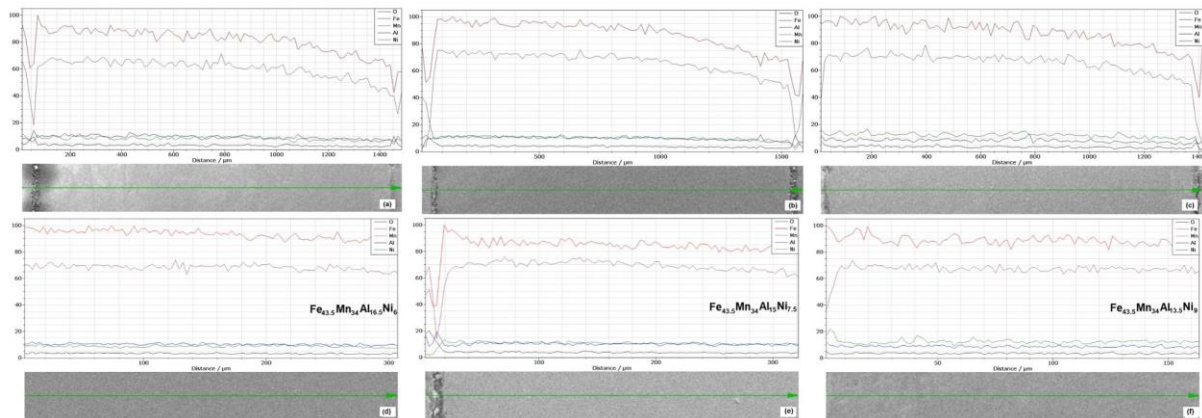


**Figure 3.** SEM-EDS line-scans at specimens in hot rolled condition: (a)  $\text{Fe}_{43.5}\text{Mn}_{34}\text{Al}_{16.5}\text{Ni}_6$ ; (b)  $\text{Fe}_{43.5}\text{Mn}_{34}\text{Al}_{15}\text{Ni}_{7.5}$  and (c)  $\text{Fe}_{43.5}\text{Mn}_{34}\text{Al}_{13.5}\text{Ni}_9$  and in annealed condition: (d)  $\text{Fe}_{43.5}\text{Mn}_{34}\text{Al}_{16.5}\text{Ni}_6$ ; (e)  $\text{Fe}_{43.5}\text{Mn}_{34}\text{Al}_{15}\text{Ni}_{7.5}$  and (f)  $\text{Fe}_{43.5}\text{Mn}_{34}\text{Al}_{13.5}\text{Ni}_9$ .

Therefore, by simple mechanical grinding over a depth of 0.1 mm on both frontal surfaces of the specimens, the oxidized layer was removed.

The typical OM micrographs, with characteristic insets, are shown in Figure 4 which summarizes all the representative microstructural particularities of the three alloys under study.

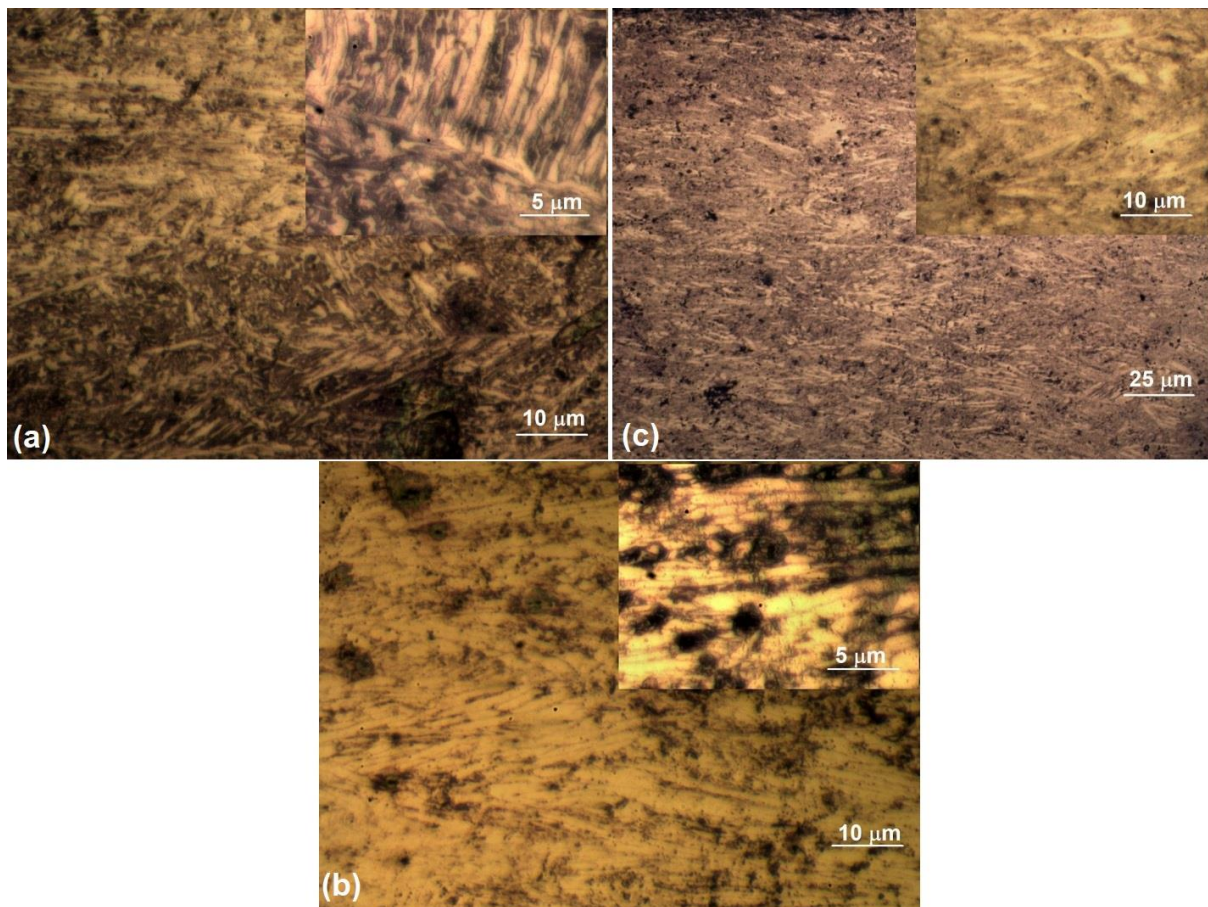


**Figure 4.** Typical OM micrographs with inset details of the specimens in cold rolled state: (a)  $\text{Fe}_{43.5}\text{Mn}_{34}\text{Al}_{16.5}\text{Ni}_6$ ; (b)  $\text{Fe}_{43.5}\text{Mn}_{34}\text{Al}_{15}\text{Ni}_{7.5}$  and (c)  $\text{Fe}_{43.5}\text{Mn}_{34}\text{Al}_{13.5}\text{Ni}_9$ .

By summarizing the results OM analysis of the three specimens passing through the first three processing steps, hot rolling, annealing and cold rolling, as compared to “classical”  $\text{Fe}_{43.5}\text{Mn}_{34}\text{Al}_{15}\text{Ni}_{7.5}$  alloy:

- $\text{Fe}_{43.5}\text{Mn}_{34}\text{Al}_{16.5}\text{Ni}_6$  have large  $\alpha$ -bcc grains with allotriomorph  $\gamma$ -fcc islets and arrays of parallel martensite plates are noticeable in the inset of Figure 3(a);
- $\text{Fe}_{43.5}\text{Mn}_{34}\text{Al}_{13.5}\text{Ni}_9$  display elongated  $\gamma$ -fcc grains that cause fibering structure after cold rolling.

As previously reported [7], fibering could be the cause of higher stiffness of specimen  $\text{Fe}_{43.5}\text{Mn}_{34}\text{Al}_{15}\text{Ni}_{7.5}$  which sustained larger stresses, displayed larger initial recoverable strain and lower permanent strain, as compared to the other two.

#### 4. Conclusions

As compared to “classic”  $\text{Fe}_{43.5}\text{Mn}_{34}\text{Al}_{15}\text{Ni}_{7.5}$ , the microstructure of  $\text{Fe}_{43.5}\text{Mn}_{34}\text{Al}_{16.5}\text{Ni}_6$  alloys consisted of  $\alpha$  – bcc phase, stabilized by the higher amount of Al, while that of  $\text{Fe}_{43.5}\text{Mn}_{34}\text{Al}_{13.5}\text{Ni}_9$  alloys comprised  $\gamma$ -fcc grains.

At  $\text{Fe}_{43.5}\text{Mn}_{34}\text{Al}_{15}\text{Ni}_{7.5}$  an obvious fibering structure was developed after cold rolling that could explain the highest stiffness, as compared to the other two specimens.

Simple mechanical grinding enabled to completely remove oxygen contamination caused by hot rolling and annealing without protective atmosphere.

A larger amount of accumulation untransformed stress-induced martensite was observed at specimen  $\text{Fe}_{43.5}\text{Mn}_{34}\text{Al}_{16.5}\text{Ni}_6$  the tensile curves of which displayed inflection points, typical to superelastic behaviour.

The presence of inflection points on the loading portions of specimen  $\text{Fe}_{43.5}\text{Mn}_{34}\text{Al}_{16.5}\text{Ni}_6$ , in Figure 1(a), confirms the repetitive occurrence of stress induced martensitic transformation and reinforces the hypothesis the gradual increase of permanent strain is caused by martensite accumulation and not by plastic deformation, during mechanical cycling.

#### 5. References

- [1] Omori T, Ando K, Okano M, Xu X, Tanaka Y, Ohnuma I, Kainuma R and Ishida K 2011 *Science* **333** 68-71
- [2] Tseng L W, Ma J, Hornbuckle B C, Karaman I, Thompson G B, Luo Z P and Chumlyakov Y I 2015 *Acta Mater.* **97** 234–244
- [3] Ueland S M, Chen Y and Schuh C A 2012 *Adv. Funct. Mater.* **22** 2094-2099
- [4] Duerig T W and Zadno R 1990 *Engineering Aspects of Shape Memory Alloys*, Duerig T W, Melton K N, Stockel D and Wayman C M (Eds.) (Oxford: Butterworth-Heinemann) pp 369-393
- [5] Oliveira J P, Zeng Z, Berveiller S, Bouscaud D, Braz Fernandes F M, Miranda R M and Zhou N 2018 *Mater. Design.* **148** 145–152
- [6] Tseng L W, Ma Ji, Vollmer M, Krooss P, Niendorf T and Karaman I 2016 *Scripta Mater.* **125** 68-72
- [7] Popa M, Pricop B, Mihalache E, Cojocaru V D, Comănesci R I and Bujoreanu L G 2019 *Mater Today Proc., special issue Bramat 2019*, to be published

#### Acknowledgments

This research work was supported by UEFISCDI through project code PN III-P4-ID-PCE-2016-0468, Contract no. 76/12.07.2017